

Original Article

Patient derived models of bladder cancer enrich the signal of the tumor cell transcriptome facilitating the analysis of the tumor cell compartment

Michalis Mastri¹, Swathi Ramakrishnan², Shruti D Shah², Ellen Karasik², Bryan M Gillard², Michael T Moser², Bailey K Farmer³, Gissou Azabdaftari⁴, Gurkamal S Chatta³, Anna Woloszynska², Kevin H Eng^{1,5}, Barbara A Foster², Wendy J Huss^{6,7}

Departments of ¹Cancer Genetics and Genomics, ²Pharmacology and Therapeutics, ³Medicine, ⁴Pathology, ⁵Biostatistics and Bioinformatics, ⁶Cell Stress Biology, ⁷Dermatology, Roswell Park Comprehensive Cancer Center, Buffalo 14263, NY, USA

Received June 10, 2021; Accepted August 6, 2021; Epub December 15, 2021; Published December 30, 2021

Abstract: The evolving paradigm of the molecular classification of bladder cancer requires models that represent the classifications with less heterogeneity. Robust transcriptome based molecular classifications are essential to address tumor heterogeneity. Patient derived models (PDMs) are a powerful preclinical tool to study specific tumor compartments. We tested if the consensus molecular subtype analysis was applicable to PDMs and evaluated the tumor compartment each model represents. PDMs derived from surgical specimens were established as xenografts (PDX), organoids (PDO), and spheroids (PDS). The surgical specimens and PDMs were molecularly characterized by RNA sequencing. PDMs that were established in immune deficient mice or *in vitro* significantly downregulated transcripts related to the immune and stromal compartments compared to the surgical specimens. However, PDMs upregulate a patient-specific bladder cancer cell signal which allowed for analysis of cancer cell pathways independent of the tumor microenvironment. Based on transcriptomic signatures, PDMs are more similar to their surgical specimen than the model type; indicating that the PDMs retained unique features of the tumor from which the PDM was derived. When comparing models, PDX models were the most similar to the surgical specimen, while PDO and PDS models were most similar to each other. When the consensus molecular subtype classification system was applied to both the surgical samples and the three PDMs, good concordance was found between all samples indicating that this system of classification can be applied to PDO and PDS models. PDMs reduce tumor heterogeneity and allow analysis of tumor cells while maintaining the gene expression profile representative of the original tumor.

Keywords: Bladder cancer, patient derived models, xenograft, organoid, spheroid, epithelial to mesenchymal transition (EMT)

Introduction

In 2021, over 80,000 new patients are predicted to be diagnosed with bladder cancer with 17,200 estimated deaths [1]. The majority of cases are non-muscle invasive bladder cancer (NMIBC) and are treated by cystoscopic resection, with or without intravesical medical therapy instilled directly into the bladder. However, approximately a third of newly diagnosed bladder cancers are muscle-invasive bladder cancer (MIBC). Therapy for these patients consists of either a radical cystectomy or definitive chemoradiation therapy. Even with definitive

treatment, the mortality from MIBC remains high. Platinum-based chemotherapy continues to be the mainstay of systemic therapy for MIBC. Overall survival remains poor, even though outcome is improved with the use of gemcitabine/cisplatin (G/C) neoadjuvant therapy [2]. With the exponential increase in knowledge about the molecular taxonomy of bladder cancer, additional therapeutic modalities are being rapidly developed and need to be tested in pre-clinical models. Several studies demonstrate that PDX models largely retain the same transcriptome, mutations and biological responses to therapies as the surgical specimen from

which they were derived [3-5]. PDXs can be used to evaluate the biological response to therapeutic agents and molecular manipulations [3, 5-7]. Studies examining PDXs and PDOs from bladder and colorectal carcinoma demonstrated that the models maintained similar drug response when compared with the patient response and had similar genomic mutation and transcriptome profiles [8, 9].

The recent development of a “consensus” molecular subtype for MIBC allows classification in the clinic to predict more effective treatment options [10]. The six molecular subtypes in the consensus molecular classification, are based on transcriptomic analysis of 1750 MIBC samples from 6 datasets. The classifications arranged from the most to least differentiated are: Luminal Papillary (LumP) 24%, Luminal Non-Specified (LumNS) 8%, Luminal Unstable (LumU) 15%, Stroma-rich 15%, Basal/Squamous (Ba/Sq) 35%, and Neuroendocrine-like (NE-like) 3% [10]. The LumP and Ba/Sq represent the most common subtypes and account for 59% of MIBC cases. LumP and Ba/Sq subtypes are at opposite ends of the spectrum of differentiation. The median overall survival is highest for the more differentiated LumP subtype, whereas the median overall survival for patients with the less differentiated Ba/Sq subtype is very poor [10]. However, validation of prognostic stratification by subtype has been inconsistent in independent studies [11]. There are several weaknesses of performing molecular analysis using bulk tissue. Tissue is comprised of multiple components including the tumor cells, stroma, and immune compartments. With bulk RNA sequencing approaches, the contribution to the overall transcriptome of individual tissue components is unclear and increases the risk that signals from rare cell populations are masked. The ESTIMATE algorithm was developed by Yoshihara et al. [12], to analyze tumor signal in a heterogeneous tumor by eliminating the immune and stroma signals.

We evaluated if the process of establishing PDMs was biased for the growth of certain cell types and if PDMs maintain the transcriptome of the tumor cell to allow comparison with the molecular subtype of the surgical specimen. PDM analysis allows detection of transcriptional changes in tumor cell populations within a heterogeneous tumor in pre-clinical studies.

Materials and methods

Ethics statement

All of the tissue samples were collected with written consent obtained prior to the collection of specimens under an Institutional Review Board (IRB)-approved protocol at Roswell Park Comprehensive Cancer Center under protocol I115707. Animal experiments were conducted and approved under our Institutional Animal Care and Use Committee (IACUC) protocol at Roswell Park.

Human specimen procurement

Human bladder tumor tissue was obtained from Roswell Park Comprehensive Cancer Center. Patients were consented for the use of remnant tissue prior to surgery. Specimens were included in these studies, provided that the tumor tissue was not needed for diagnostic purposes. Patients who declined consent or were unable to consent were excluded from these studies. Inclusion criteria were bladder tumors of all stages, pathology, and treatment history from which a minimal of 100 mg of fresh remnant tissue was available for distribution. Fresh human bladder tissues were procured from transurethral resection of bladder tumor (TURBT) or radical cystectomies undergoing diagnostic and therapeutic resection of bladder tumors. Specimens from TURBT procedures were from portions of the tumor in the bladder lumen. Specimens from cystectomies were reviewed by a pathologist as remnant tissue not needed for diagnosis. Remnant tissue from tumor specimens was obtained from the Pathology Network Shared Resource at Roswell Park under an approved IRB protocol. Tissues were stored in static preservation solution (Belzer UW® Cold Storage Solution, Bridge to Life) up to 16 hours at 4°C. De-identified demographics (clinical stage, procedure, gender, age, ethnicity, smoking status, and treatment prior to specimen collection) were obtained from Biomedical Research Informatics Shared Resource at Roswell Park.

Patient derived models

Xenograft generation: The Experimental Tumor Model Shared Resource at Roswell Park received patient samples for grafting into sex matched NOD.Cg-Prkdc^{scid} Il2r^{tm1Wjl}/SzJ mice

Bladder cancer patient derived models enrich tumor cell transcriptome signal

Table 1. Spheroid and organoid media components

Material	Source	Product number	PDS conc.	PDO conc.
Base Media	Invitrogen	12637-010	-	Advanced DMEM
	Invitrogen	11320-033	DMEM/F12	-
B27	Invitrogen	17504-044	2× diluted	50× diluted
N-acetylcysteine	Sigma	A9165	-	1.25 mM
EGF	Peprotech	AF-100-15	10 ng/ml	5 ng/ml
Noggin	Peprotech	120-10C	-	100 ng/ml
R-spondin 1	R&D Systems	4645-RS-025	-	500 ng/ml or 10% conditioned medium
A83-01	Tocris Bioscience	2939	-	500 nM
FGF10	Peprotech	100-26	-	10 ng/ml
FGF2	Peprotech	100-18B	5 ng/ml	5 ng/ml
Prostaglandin E2	Tocris Bioscience	2296	-	1 μM
Nicotinamide	Sigma	N0636	-	10 mM
SB202190	Sigma	S7076	-	10 μM
Insulin	Invitrogen	12585-014	-	4 mg/ml
Y-27632 dihydrochloride	Selleck Chemical	S1049	-	10 μM

(JAX, Bar Harbor, ME) hosts, also known as NOD SCID gamma (NSG). Patient samples that grew in NSG hosts are designated as p0, and the next passage in NSG hosts is p1, and so on. Bladder tumor pieces (0.5-1 mm³) were dipped in Matrigel® (#354234, Corning) and grafted subcutaneously into the flank of host NSG mice. From each patient sample, 5 sex matched NSG hosts were grafted with 2 pieces of patient tumors, the number of hosts grafted occasionally varied between 4 and 6, as determined by patient tumor size and host animal availability. PDX-p0s that grew from the patient sample were harvested when tumor volume reached 1.5 cm³ and 1 tumor piece was grafted per host, into 5 host animals to expand the PDX by three additional rounds of growth (p1, p2, p3). Mice were housed in a limited access barrier facility within the Laboratory Animal Shared Resource (LASR), in ventilated cages under standard conditions with food and water available ad libitum. All animal studies were conducted in accordance with the recommendations in the Guide for the Care and Use of Laboratory Animals. Roswell Park is an AAALAC International Accredited Animal Program.

Organoid and spheroid generation and culture:

Tumor tissue from surgical specimens and tumors from PDX models (p2-3) was minced and enzymatically digested in a modified protocol previously published [13, 14]. Briefly, samples are incubated in a collagenase II (0.28%, #1148090, Sigma), dispase (2.4 Units/mL, #17105-041, ThermoFisher) and DNA-

se (0.01%, #10104159001, Sigma) solution in DPBS (#14190-144, Invitrogen) in a 50 mL flask for 1-2 hours at 37°C with gentle stirring. If necessary, red blood cells are removed by lysis using RBC lysis buffer, epithelial cells were isolated with a Histopaque gradient (#10771, Sigma) and plated for 3D culture as previously described [14]. Single cells were passed through a 100 μm cell strainer and resuspended in media appropriate for generation of organoids [15] or spheroids [16, 17] (**Table 1**).

For organoid growth, viable suspended cells were cultured in 5% Matrigel in defined organoid media using the base R-spondin organoid culture system [15] with growth factor conditions adapted for use with urothelial TCC (**Table 1**). PDSs and PDOs were expanded at a low passage rate of 2-4 after a dispase digestion (2.4 Units/ml in DPBS) of Matrigel followed by PDO digestion by TrypLE Express (#126040-13, ThermoFisher Scientific). Spheroids were established by seeding 1×10³ viable single cells/well in 24-well, ultra-low adhesion plates (#734-2779, VWR) in 5% Matrigel in defined spheroid media. Once PDOs and PDSs reached p2 growth in multiple wells, aliquots were frozen for RNA sequencing.

Authentication of models and patient surgical samples:

Short tandem repeats (STR) profiles were performed by Roswell Park's Genomic Shared Resource to authenticate that PDXs were derived from the matching patient sample. Flash frozen patient tumor samples were

Bladder cancer patient derived models enrich tumor cell transcriptome signal

collected at the time of procurement and sent to the Genomic Shared Resource for DNA isolation and STR profile analysis. AmpFLSTR® Identifiler® Plus PCR Amplification Kit (#4486-467, ThermoFisher Scientific) was used for STR profiling which utilizes fifteen STR loci and the sex-determining marker Amelogenin. PDX STR profile was compared to the patient tumor STR profile. A match of patient and PDM was called if the STR profile had a $\geq 90\%$ match.

Histology and immunohistochemistry (IHC)

PDX tissues were formalin fixed and embedded in paraffin with the Leica ASP300S processor. Serial sections (5 μm) were cut and mounted on glass slides (#MER7255/90/WH, Mercedes Medical). Slides were deparaffinized in xylene, rehydrated through a graded series of alcohol washes, and equilibrated in double distilled water. Slides were stained with Hematoxylin and Eosin (H&E) using a DAKO Coverstainer. Immunohistochemistry was performed using a DAKO PT link. Slides were incubated in 1 \times pH6 citrate buffer (#00-5000, Invitrogen) for 20 minutes, then for incubation in 3% H₂O₂ (#88597, Sigma) for 15 min. To block non-specific binding, tissues were incubated with 10% normal goat serum (#50062Z, Invitrogen) for 10 min, followed by avidin/biotin block (#SP-2001, Vector Labs). Primary antibodies of E-cadherin (1:500 dilution, #610181, BD Biosciences), cytokeratin 5 (CK5) (1:1000 dilution, #PRB 160p, Covance), cytokeratin 20 (CK20) (1:500 dilution, #ab97511, Abcam), synaptophysin (1:400 dilution, #ab52636, Abcam) and vimentin (1:400 dilution, #5741, Cell Signaling) were diluted in 1% BSA solution (#BP1605-100, ThermoFisher Scientific) and incubated for 30 minutes at room temperature. All of the slides were incubated with the goat anti-rabbit biotinylated secondary antibody (1:600 dilution, #BA1000, Vector Biolabs) for 15 minutes at room temperature. For signal enhancement, ABC reagent (#PK 6100, Vector Biolabs) was applied for 30 minutes. To reveal peroxidase activity, slides were incubated with 3,3'-Diaminobenzidine (DAB) (#K3467, DAKO) substrate for 5 minutes and counterstained with DAKO Hematoxylin (#CS7000, DAKO) for 20 seconds. All slides were imaged with the Aperio AT2 Scanner (Leica) at 20 \times and analyzed with Aperio Imagescope software (Leica).

RNA isolation and sequencing

RNA/DNA extraction was performed in the Genomics Shared Resource at Roswell Park. The purification of total RNA was prepared using the miRNeasy micro kit (#217084, Qiagen). Frozen tissues, organoid suspensions, and spheroid suspension samples were first suspended in 700 μl of Qiazol reagent. The samples were homogenized using Navy Rhino tubes in a Bullet Blender Homogenizer (Next Advance) for 5 minutes. The homogenate was removed and incubated in a new tube at room temperature. After addition of chloroform, the homogenate was separated into aqueous and organic phases by centrifugation. RNA partitions to the upper aqueous phase, while DNA partitions to the interphase and proteins to the lower organic phase or the interphase. The upper, aqueous phase was extracted, and ethanol added to bind RNA molecules of 18 nucleotides and larger. The sample was applied to the miRNeasy micro spin column, where the total RNA bound to the membrane and phenol and other contaminants were efficiently washed away. On-column DNase digestion was performed to remove any residual genomic DNA contamination followed by additional washes. High quality RNA was eluted in 25 μl of RNase-free water. Quantitative assessment of the purified total RNA was accomplished by using a Qubit High Sensitivity RNA kit, and concentration determined by Ribogreen fluorescent binding to isolated RNA. The RNA was further evaluated qualitatively using RNA High Sensitivity tape on the 4200 TapeStation (Agilent technologies), where sizing of the RNA was determined and a qualitative numerical score (RINe) assigned. Amplified cDNA was generated using the SMART-Seq v4 Ultra Low Input RNA kit (#Q32852, ThermoFisher Scientific). 10 ng of total RNA was fragmented based on % DV200 analysis and used to synthesize first-strand cDNA utilizing proprietary template switching oligos. Amplified double strand (ds) cDNA was created by LD PCR using blocked PCR primers with incorporation of unique sample barcodes. The resulting ds cDNA was purified using Ampure XP beads (#A63881, Beckman Coulter). Abundant Ribosomal cDNA was depleted using R probes, and 13 cycles of PCR using universal PCR primers to complete the library. The final libraries were purified using Ampure XP beads and validated for appropriate size with

Bladder cancer patient derived models enrich tumor cell transcriptome signal

Screening on the TapeStation. The libraries were quantitated using KAPA Biosystems qPCR kit (#KRO397, Sigma) and were pooled together in an equimolar fashion following experimental design criteria. Each pool was denatured and diluted to 400 pM with 1% PhiX control library. The resulting pool was loaded into 200 cycle NovaSeq Reagent cartridge for 2×100 sequencing on a NovaSeq6000 following the manufacturer's recommended protocol (Illumina Inc.).

Bioinformatics and statistical analysis

RNA data processing: Sequencing quality control was assessed using FASTQC v0.11.5 (available online at: <http://www.bioinformatics.babraham.ac.uk/projects/fastqc/>). Reads were aligned to the human genome GRCh38 release 27 (GenCode) using STAR v2.6.0a [18] and post-alignment quality control was assessed using RSeQC v2.6.5 [19]. Aligned reads were quantified at the gene level using RSEM v1.3.1 [20]. RSEM estimated gene counts were filtered and upper quartile normalized using the R-based Bioconductor package edgeR [21]. Differential gene expression was performed after voom transformation followed by linear regression using the R-based Bioconductor package Limma [22]. Genes with a fold change greater than 2 and adjusted *p*-value of less than 0.05 were considered to be statistically significant differentially expressed.

Euclidean distance calculations: For t-distributed stochastic neighbor embedding (t-SNE) we defined Euclidean distance based on the expression of a subset of genes. Genes were selected based on the average expression in all PDM and surgical specimens. Genes highly expressed in PDMs compared to surgical specimens were chosen in order to eliminate genes related to immune or other tumor microenvironment cells. t-SNE plots were made using the R-based package Rtsne (<https://github.com/jkrijthe/Rtsne>) [23-25].

Hallmark Gene Set, EMT, consensus molecular subtype analysis: Gene set enrichment analysis was performed using the R-based Bioconductor package fgsea [26] for the hallmark gene sets from the molecular signatures database (MSigDB) [27, 28]. Molecular subtype classifications were performed on all surgical and PDM specimens using the consensus MIBC

R package [29]. Using RNA sequencing data, molecular subtype was assigned to samples only when the correlation value was greater than 0.3. The consensus MIBC R package can identify 6 molecular classes: Luminal Papillary (LumP), Luminal Non Specified (LumNS), Luminal Unstable (LumU), Stroma-rich, Basal/Squamous (Ba/Sq), and Neuroendocrine-like (NE-like).

Statistical analysis

Statistical analysis was performed using R v.4.0.2 through RStudio v.1.3.1073 (Integrated Development for R; Rstudio, Inc., Boston, MA). Moderated t-tests were used for differentially expressed genes through limma R package and fishers exact test was used for enrichment test. A minimum significance level of 0.05 was used for all analyses after adjustment for multiple comparisons using false discovery rate.

Results

PDMs established from surgical specimens of bladder cancer

The ability of tumor specimens to grow and establish a PDX model was determined by implanting 55 freshly procured bladder tumor specimens from TURBT or cystectomy procedures at Roswell Park (**Table 2**). Nineteen (19) of 55 specimens grafted into sex-matched NSG host animals demonstrated tumor growth of at least 1 cm³ in the initial passage (34.5%; 95% CI: 21.6-47.5%). Initial growth of the grafted surgical specimen is considered p0. Nine (9) of the 19 tumors with initial growth (47.4%, 95% CI: 22.6-72.1%) established PDX tumor lines defined as established growth beyond p2 and demonstrated >80% tumor take rate after a viable freeze. Thus, 9 PDX tumor lines have been established from 55 patient specimens for a 16.4% (95% CI: 6.3-26.5%) overall take-rate, similar to previous studies [3, 9, 30, 31]. In **Table 3**, the histopathology and de-identified demographic information of the patient tumor specimens, specimens that established PDX models are highlighted. Surprisingly, there was no correlation between the ability to establish PDX models and tumor stage or treatment. Of note, even a T1 staged surgical specimen (RP-BL040) was able to establish a PDX. Interestingly, specimens from female patients were more likely to establish models at p0 com-

Bladder cancer patient derived models enrich tumor cell transcriptome signal

Table 2. Patient demographics for all specimens where PDMs were attempted, shaded specimens with established >p3 PDX models

RP-BL	Growth	Tumor Stage	Treatment	Pathology	Procedure	Sex	Age	Ethnicity	Smoking Status
001	ND	T3	None	HG papillary urothelial carcinoma	Cystoprostatectomy	M	83	C	Never
002	No	T3	None	HG urothelial carcinoma with nested and lymphoepithelial features	TURBT	M	75	C	Never
003	Est	T3	G/C	HG urothelial carcinoma	TURBT	F	57	AA	Current
004	No	T1	BCG	HG urothelial carcinoma	TURBT	M	79	C	Former
005	Est	T2	None	HG urothelial with sarcomatoid features	TURBT	M	83	C	Former
006	No	T2	BCG	Recurrence HG urothelial carcinoma	TURBT	M	55	C	Current
007	No	T2	BCG	HG papillary urothelial carcinoma	Cystoprostatectomy	M	84	AA	Former
008	No	T1	BCG	HG papillary urothelial carcinoma	TURBT	M	68	AA	Current
009	Yes	T1	None	HG papillary urothelial carcinoma	TURBT	M	58	C	Never
010	Yes	T2	None	HG urothelial carcinoma	TURBT	F	64	C	Current
011	No-I	NA	NA	NA	NA	NA	NA	NA	NA
012	Yes	T2	None	HG urothelial carcinoma	TURBT	F	65	C	Current
013	No	T1	BCG	HG papillary urothelial carcinoma	TURBT	M	66	C	Never
014	No	T2	None	HG urothelial carcinoma	TURBT	M	81	C	Former
015	No	T3	Atezolizumab	HG urothelial carcinoma, plasmacytoid variant	Cystoprostatectomy	M	72	C	Current
016	No	T1	Atezolizumab	HG papillary urothelial carcinoma	TURBT	F	85	C	Former
017	No	T2	None	HG papillary urothelial carcinoma	TURBT	M	67	C	Former
018	No	T2	Pembro	HG papillary urothelial carcinoma	TURBT	M	63	C	Current
019	Est	T3	G/C	HG urothelial carcinoma	Cystectomy	F	66	C	Former
020	No	T1	None	HG papillary urothelial carcinoma	TURBT	M	68	C	Former
021	Yes	T1	None	HG papillary urothelial carcinoma	TURBT	M	84	C	Never
022	Est	T2	G/C	HG papillary urothelial carcinoma	TURBT	M	76	C	Former
023	No	T2	BCG	HG papillary urothelial carcinoma	Nephroureterectomy	M	72	C	Never
024	No	T2	None	HG urothelial carcinoma with predominantly sarcomatoid	Cystoprostatectomy	M	75	C	Former
025	No	NA	ADT	Prostate adenocarcinoma	TURBT	M	67	AA	Never
026	Yes	T4	None	HG urothelial carcinoma	Cystectomy	F	69	C	Current
027	No	T4	None	HG urothelial carcinoma	Cystoprostatectomy	M	72	C	Former
028	No	NA	Multiple Chemo	Metastatic colon adenocarcinoma	TURBT	M	70	C	Never
029	Yes	T1	BCG+INF	HG papillary urothelial carcinoma	Cystoprostatectomy	M	46	C	Current
030	Yes	T1	Treatment for Multiple Myeloma	HG urothelial carcinoma	TURBT	M	83	C	Former
031	No	T1	None	HG papillary urothelial carcinoma	Cystoprostatectomy	M	84	C	Never
032	No	T1	None	HG urothelial carcinoma with squamous differentiation	TURBT	M	86	C	Never
033	No	T1	None	HG urothelial carcinoma	TURBT	M	52	C	Former
034	No	T4	None	HG urothelial carcinoma with focal glandular and squamous differentiation	TURBT	M	64	C	Never
035	No	T2	None	HG urothelial carcinoma	TURBT	M	84	C	Former
036	Yes	T1	None	HG papillary urothelial carcinoma	TURBT	M	76	C	Former
037	Yes	T1	None	HG papillary urothelial carcinoma	TURBT	M	52	C	Former
038	No	T1	None	HG papillary urothelial carcinoma	TURBT	M	75	C	Former

Bladder cancer patient derived models enrich tumor cell transcriptome signal

039	No	T1	None	HG papillary urothelial carcinoma	TURBT	M	76	C	Current
040	Est	T1	None	HG urothelial carcinoma with prominent squamous differentiation	TURBT	F	72	C	Never
041	No	T2	None	HG papillary urothelial carcinoma	TURBT	M	>89	C	Former
042	No	T2	G/C	HG papillary urothelial carcinoma with focal squamous differentiation	TURBT	M	76	C	Never
043	No	T2	None	Poorly differentiated urothelial carcinoma w/basal-squamous differentiation	TURBT	M	47	C	Former
044	No	Ta	None	HG papillary urothelial carcinoma	TURBT	M	68	C	Current
045	Yes	T2	G/C	HG papillary urothelial carcinoma	TURBT	M	76	C	Never
046	No	T1	None	HG urothelial carcinoma	TURBT	M	54	C	Current
047	No	T1	None	HG papillary urothelial carcinoma	TURBT	F	82	C	Former
048	No	T2	None	HG papillary urothelial carcinoma	Cystoprostatectomy	M	51	C	Current
049	No	T4	Pembro	HG papillary urothelial carcinoma	TURBT	M	79	C	Former
050	Est	T3	None	HG urothelial carcinoma with squamous differentiation	TURBT	F	76	C	Never
051	Est	T3	None	HG papillary urothelial carcinoma	TURBT	M	61	C	Never
052	Est	T3	BCG, G/C, pembro	Recurrence, HG papillary urothelial carcinoma	TURBT	F	64	C	Former
053	No-I	NA	NA	NA	NA	NA	NA	NA	NA
054	Est	T2	None	HG papillary urothelial carcinoma	TURBT	F	85	C	Never
055	No	T2	None	HG urothelial carcinoma w/squamous diff	Cystoprostatectomy	F	75	C	Current
056	No	T3	None	HG urothelial carcinoma w/squamous diff	TURBT	F	73	C	Former

BCG = Bacillus Calmette-Guerin; G/C = Gemcitabine/Cisplatin; INF = Interferon; Pembro = pembrolizumab; ADT = Androgen Deprivation Therapy; HG = high grade; TURBT = Transurethral Resection Bladder Tumor; F = Female; M = Male; C = Caucasian; AA = African American; ND = Not determined; NA = Not available. Growth column: Est = Established PDX model; Yes = Grew but did not establish passable PDX model; No = No Growth; No-I = No Growth, all grafted animals died due to infection. Row shading indicates surgical specimen that established PDXs and are also in **Table 3**.

Table 3. Histopathology and molecular subtypes of surgical specimens and PDMs

RP-BL Line	Histopathology		Molecular Subtype			
	Surgical Specimen	PDX	Surgical Specimen	PDX	PDO	PDS
051	HG papillary urothelial carcinoma	HG papillary urothelial carcinoma with squamous diff	Ba/Sq	Ba/Sq	ND	ND
050	HG urothelial carcinoma with squamous differentiation	HG papillary urothelial carcinoma with squamous diff	Ba/Sq	Ba/Sq	ND	ND
040	HG with prominent squamous differentiation	HG papillary urothelial carcinoma with squamous diff	Ba/Sq	Ba/Sq	ND	ND
005	HG urothelial with sarcomatoid features	HG papillary urothelial carcinoma with sarcomatoid	Ba/Sq	Ba/Sq	Ba/Sq	Ba/Sq
054	HG papillary urothelial carcinoma	HG papillary urothelial carcinoma with squamous diff and sarcomatoid	Ba/Sq	Ba/Sq	LumP	Ba/Sq
003	HG urothelial carcinoma	HG papillary urothelial carcinoma with squamous diff	Ba/Sq	LumP	LumP*	LumP*
019	HG urothelial carcinoma	HG papillary urothelial carcinoma with predominately sarcomatoid	LumP	LumP	LumP	LumP
022	HG papillary urothelial	NE differentiation	LumP	LumP	LumP	LumP

ND-Not Determined the unique mapped reads (<1.1%) and low RNA yield (<30 ng) for RP-BL051 PDO and was not analyzed, PDXs were sequenced at passage 2, PDO and PDS models are derived from the sequenced PDX. *, The PDMs derived from RP-BL003 were derived and sequenced from PDX at passage 3.

pared to specimens from male patients (69.2% versus 23.8%, t-test of proportions $P=0.0075$), independent of tumor stage. PDOs and PDSs were established from either surgical specimens when enough surgical sample was available or from PDX tumors to provide *in vitro* tools for future analysis. Due to the small size of the majority of surgical samples, only RP-BL019 and RP-BL022 have a PDO and RP-BL022 has a PDS derived directly from the surgical specimen. However, PDOs and PDSs were able to be established from the patient's PDX and were used to evaluate sample variability due to model section conditions vs. patient tumor.

Molecular comparison of PDMs with original surgical specimen

PDM transcriptomes faithfully represent their corresponding surgical specimen: To determine whether gene expression changes are associated with specific types of PDMs, the transcriptome from each PDM was analyzed individually to identify differences between each patient's surgical specimen and their corresponding model (**Figure 1**). The Euclidian distance between all the samples was calculated after filtering out genes that are underrepresented or not expressed in the PDMs, such as genes expressed by immune cells and fibroblast. Using the Euclidian distance between the samples and the t-distributed stochastic neighboring embedding algorithm to visualize how similar the samples are, PDMs clustered with their corresponding surgical specimen (**Figure 1A**). This clustering was persistent even when 3D cultures (defined as PDO and PDS) (**Figure 1B**), surgical specimens (**Figure 1C**), or surgical specimen and PDX (**Figure 1D**) were removed from the analysis. Interestingly, PDO and PDS derived from PDX tumor specimens, and not directly from the surgical specimen, still clustered with their patient surgical specimen. Euclidean distance based on gene expression showed that PDX models are the most similar to the surgical specimens followed by PDO and finally PDS (**Figure 1E**). We identified differentially expressed genes by paired comparison of each PDM to its corresponding surgical specimen (**Figure 1F**). This confirmed that PDXs are the most similar to surgical samples, whereas PDOs and PDSs are more similar to each other than surgical specimens or PDX.

PDMs enrich the tumor compartment transcriptome: To further examine the relationship between PDM and surgical specimen, differential gene expression was performed without filtering genes. Analysis between PDMs and the surgical specimens showed that 1654 genes are significantly downregulated in PDMs, whereas only 48 are upregulated (**Figure 2A**). We focused on 5 groups of genes related to tumor, bladder stem cells (BSC), general stem cells (SC), immune system, and the stroma. Only genes related to the immune system and the stroma were significantly downregulated in PDMs, indicating that PDMs are representative of the tumor compartment but not the overall tumor microenvironment. Gene expression was visualized for each surgical specimen and PDM for the 5 tumor related groups of genes (**Figure 2B**). The gene expression pattern shows the expression of the individual genes in each of the samples emphasizing that the majority of the stroma and immune related genes are under-represented in PDMs.

Hallmark gene set enrichment analysis in surgical specimens and PDMs: To further characterize the PDMs, gene set enrichment analysis for the hallmark gene sets was performed comparing surgical specimen vs. PDX, PDX vs. 3D models, and PDS vs. PDO (**Figure 3A**). The gene sets were grouped into 8 processes: development; DNA damage; immune; cellular component; metabolic; stress pathway; proliferation; and signaling. Multiple gene sets were enriched in the surgical samples compared to the PDMs, but only the immune related gene sets were over-represented in the surgical specimens (**Figure 3B**). Interestingly, gene sets in the stress pathway group (apoptosis, protein secretion, reactive oxygen species, and unfolded protein) were enriched in the 3D culture PDMs compared to the PDX (**Figure 3C**).

Transcription analysis of genes associated with EMT and molecular subtypes: EMT is a hallmark of cancer progression, generates cells with cancer stem cell properties and has been associated with poorer outcomes [32-34]. Therefore, the enrichment score for the EMT hallmark gene set was examined in the surgical samples and PDMs (**Figure 3A**). The enrichment score for the EMT gene set showed that SURG is enriched vs. PDMs, PDX is enriched vs. 3D cultures and PDS is enriched vs. PDO mod-

Bladder cancer patient derived models enrich tumor cell transcriptome signal

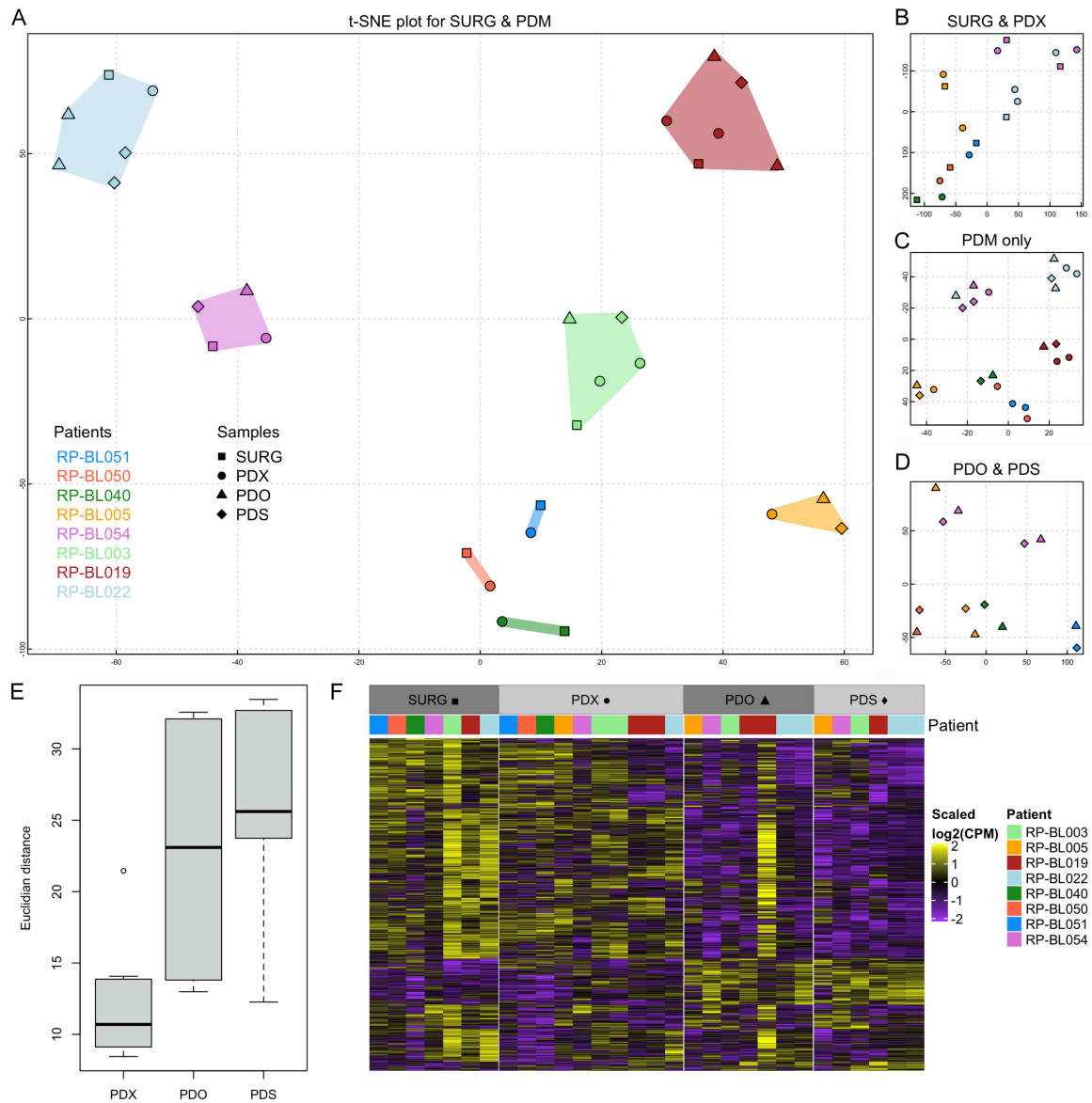


Figure 1. PDMs are a faithful representation of their original tumor. (A-D) Euclidean distance was visualized with t-SNE for (A) all samples, (B) surgical and PDX samples, (C) only PDM samples, and (D) PDO and PDS samples. (E) Euclidean distance of each PDM to their corresponding surgical specimen. (F) Heatmap of differentially expressed genes identified by paired comparison of PDM compared to their corresponding surgical specimen.

els (Figure 4A). Expression of EMT genes was not sufficient to cluster the samples by patient, indicating that other biological processes besides the EMT signature define the surgical specimen (Figure 4B). The expression level of the EMT gene set is increased in the surgical specimens compared to the PDMs (Figure 4A).

The consensus molecular subtyping was developed to molecularly classify MIBC based on transcriptomic data [10]. The consensus molecular subtype classification of MIBC was analyzed for each surgical specimen and PDM to

determine if the molecular subtype can be used to classify PDMs. The molecular subtypes were determined for seven surgical specimens and their matched PDX models, as well as six PDO and PDS models derived from the surgical specimens and PDX models (Figure 4D). The molecular subtype classification was designed for MIBC surgical specimens. In the majority of the cases (6/8, 75%), PDMs were classified as the same as the molecular subtype of their corresponding surgical specimen (Table 3), indicating that the molecular subtype classification can be useful to characterize PDMs. Of the sur-

Bladder cancer patient derived models enrich tumor cell transcriptome signal

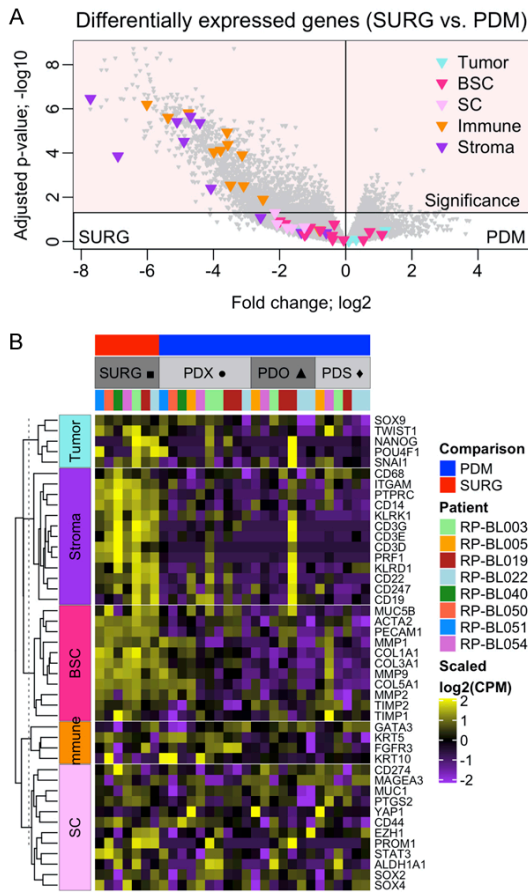


Figure 2. PDMs represent the tumor but not the tumor microenvironment. A. Volcano plots of differentially expressed genes comparing surgical specimens to PDM emphasizing the selected genes for tumor and tumor microenvironment. B. Heatmap of gene expression corresponding to tumor, bladder cancer stem cell (BSC), stem cell (SC), immune, and stroma genes.

gical specimens that established PDMs, a high percent (6/8, 75%) were classified as the Ba/Sq molecular subtype. In general, the consensus molecular subtype of the PDMs agreed with the surgical specimen.

Histopathology and differentiation marker analysis

Historically, tumor stage and histopathology provides key information used to determine stage and treatment options; however, information evaluating the histopathology, expression of differentiation markers and molecular subtypes in PDMs is limited [35]. Characterizing each model for histopathology and molecular

subtype better evaluates how closely the PDMs represent the surgical sample of the patient from which they were derived. To determine how well the consensus molecular phenotype represents the tumor histopathology, the histopathology of available surgical specimens and PDXs were evaluated by a GU pathologist. The molecular subtype was consistent between 7/8 surgical specimens and their derived PDX models. The exception was RP-BL003 in which the surgical specimen was classified as Ba/Sq and the PDX was LumP. Interestingly, the RP-BL003 PDX demonstrated a squamous differentiated histopathology but the surgical specimen did not. A high number of PDXs (5/8) had histopathologies not found in the surgical specimen. RP-BL051, -054 and -003 had squamous differentiation; RP-BL054 and 019 had sarcomatoid features; and RP-BL022 had NE differentiation (**Table 3**).

In general, the PDX histopathologies were concordant with that of the surgical specimen, although there was a trend towards the PDX being more undifferentiated with a gain of the squamous phenotype. To further elucidate the similarities and differences in the histopathology and the molecular subtype, sections of PDX tumors were analyzed by IHC to identify cells expressing the following differentiation markers: E-cadherin (epithelial marker), CK5 (basal marker), CK20 (superficial/intermediate urothelium marker), vimentin (EMT marker) and synaptophysin (NE marker) (**Figures 5 and 6**). The IHC analysis demonstrated high expression levels of CK5 in RP-BL051, RP-BL050, RP-BL040, and RP-BL054 that match the Ba/Sq molecular subtype. CK20 was highly expressed in RP-BL019 as expected based on the differentiated histopathology and LumP molecular subtype (**Figure 6**).

Discussion

In this study we compared three types of PDMs with their surgical samples to evaluate: systemic bias in the models; how well each model type represents the patient surgical sample; and if the bulk transcriptome of the PDMs can be used to analyze the tumor cell transcriptome without transcriptomic contribution from the stroma and immune compartments. The PDMs were analyzed to assess whether the type of model was more similar to each other or if the

Bladder cancer patient derived models enrich tumor cell transcriptome signal

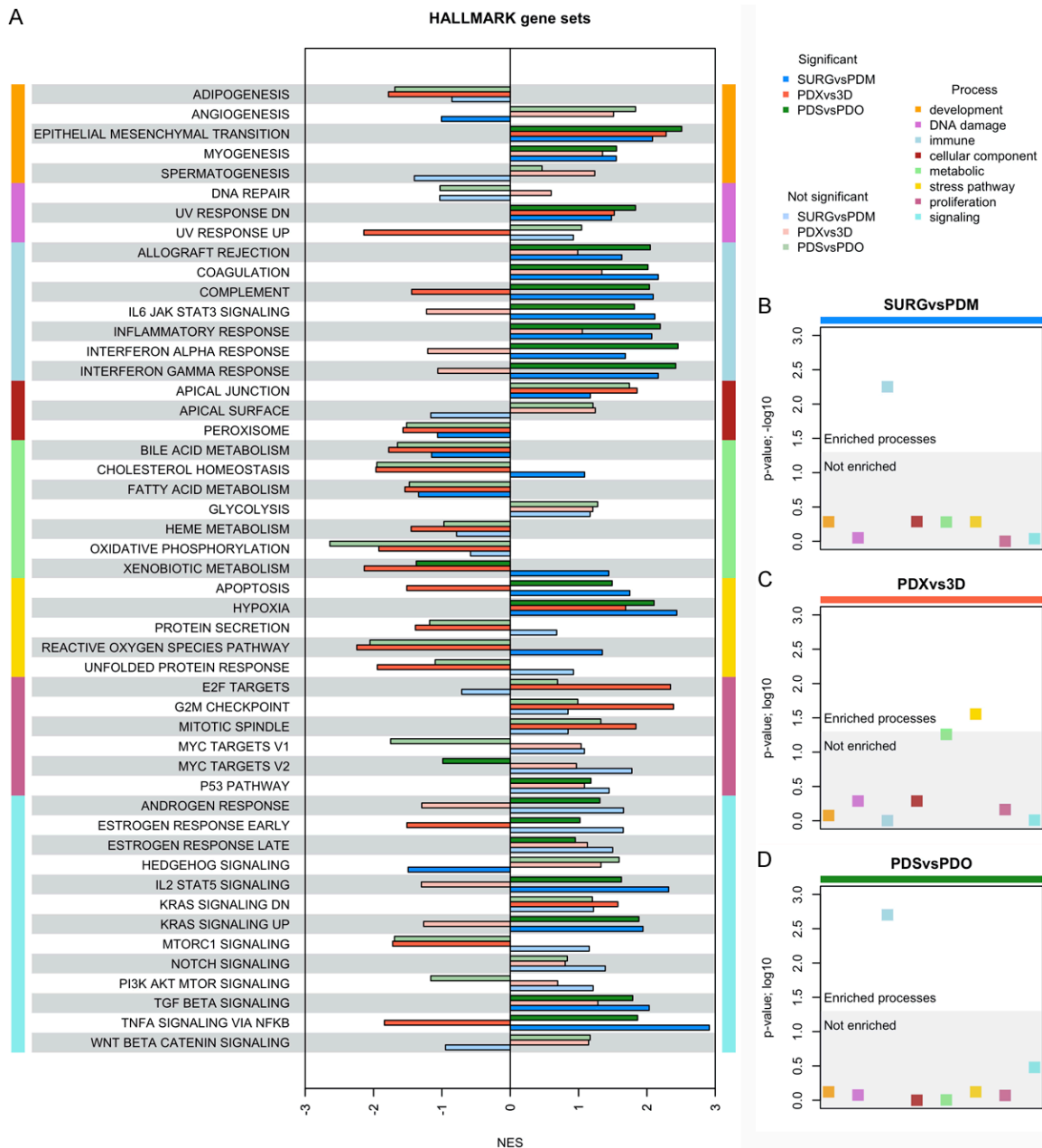


Figure 3. Hallmark pathway analysis RNAseq. (A) Gene set enrichment analysis for all the hallmark gene sets for 3 different comparisons (SURG vs. PDM, PDX vs. 3D, PDS vs. PDO). Gene sets were categorized based on processes. (B-D) Enrichment of processes based on fisher exact test for (B) SURG vs. PDM, (C) PDX vs. 3D, and (D) PDS vs. PDO.

transcriptomes of the models were more like their original surgical specimen. Interestingly, all PDMs were more similar to the surgical specimen from which they were derived (**Figure 1**). Analysis of transcriptomic data indicates that the primary driver of variability is from interpatient differences and not the type of model. Our results are consistent with our previous studies in which we demonstrated that the transcriptomes of bladder cancer cell lines

grown in 2D cell culture were comparable to xenografts of the cell line [36]. We classified the consensus molecular subtype for 8 cases of surgical sample and their PDMs. We found that in general our studies are in agreement with previous studies [11, 37], that bladder PDMs faithfully recapitulate the molecular subtype of their corresponding surgical sample and PDXs consistently reflected the histologic phenotype of their surgical sample. The few dis-

Bladder cancer patient derived models enrich tumor cell transcriptome signal

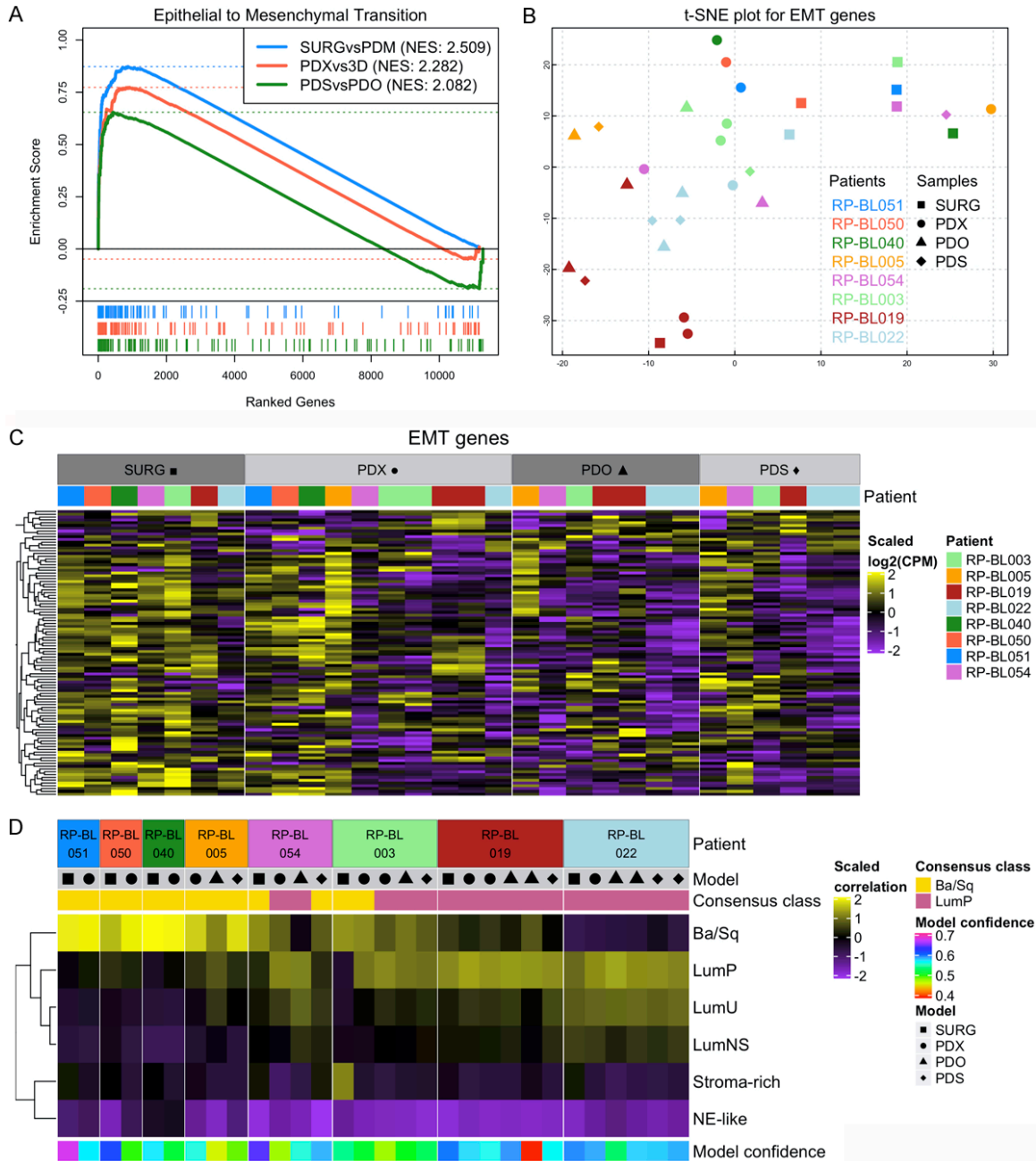
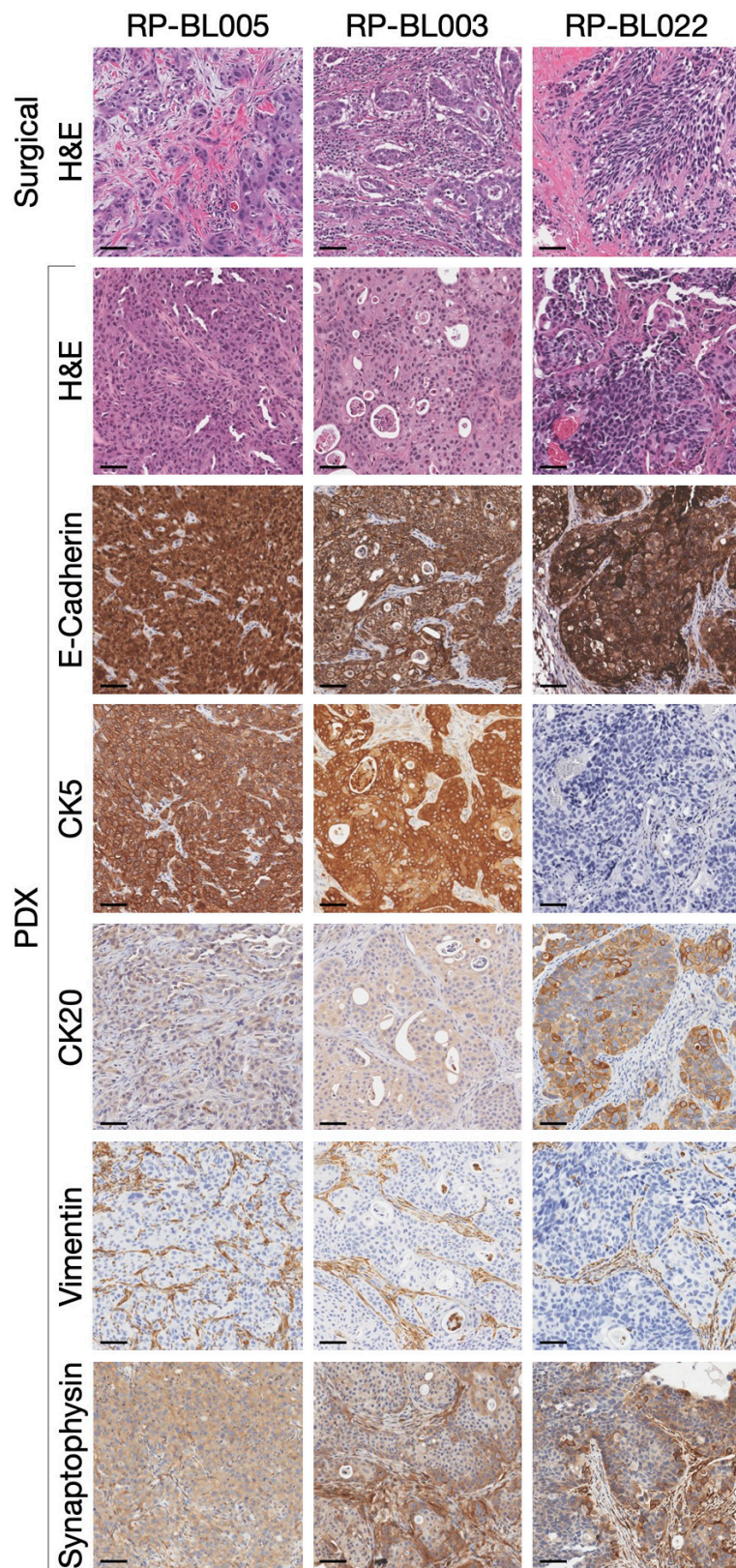


Figure 4. EMT and Ba/Sq molecular subtypes are enriched in PDMs. (A) Gene set enrichment analysis for the hallmark epithelial to mesenchymal transition gene set for 3 different comparisons (PDM vs. SURG, PDX vs. 3D, PDS vs. PDO). (B, C) Expression of the hallmark epithelial to mesenchymal transition genes were used for (B) t-SNE plot and (C) heatmap. (D) Correlation heatmap based on the consensus molecular subtype scores for each sample derived from RNA sequencing data.

crepancies in molecular subtype between the patient specimen and models can be explained due to different areas of the tumor being used to make each model as proposed by Schütte, et al. for colorectal cancer [8]. Thus, PDMs faithfully represented the transcriptomic profile of their surgical sample. Moreover, the conditions

that establish and maintain PDMs did not introduce systemic bias that skewed the transcriptome away from the surgical specimen. Thus, PDMs should be selected based on the ability to address the scientific question, since all models were representative of their original surgical specimen.

Bladder cancer patient derived models enrich tumor cell transcriptome signal



IHC analysis of PDX models for E-Cadherin, CK5, CK20, Vimentin, and Synaptophysin. Slides were imaged at 20 \times , Scale Bar =100 μ m

There was no difference in establishment of PDX models based on tumor stage, indicating cancer cells capable of establishing PDX growth are present in all tumor stages. While, 47% (9/19) tumors with initial growth established PDX tumor lines, the overall 16% (9/55) establish take-rate is low but similar to previous studies [3, 9, 30, 31]. Interestingly, T1-T2 stage surgical specimens represented 3 of the 4 highest EMT signatures found in the surgical specimens, even though EMT signatures are typically associated with higher grade, less differentiated tumors. Surgical specimens from female patients were more likely to establish models compared to specimens from male patients independent of tumor stage. There was no difference in EMT genes between PDO or PDS derived from patients that received treatment compared to those that were derived from patients that were treatment naïve. PDMs closely represent the patient surgical sample from which they were derived. Interpatient variability drives differences across models, rather than the conditions used to establish PDMs. PDMs have been established from low stage [3, 9] and muscle invasive bladder cancer [3, 9, 37, 38] and analysis focuses on how similar the models are to the original patient surgical samples.

Figure 5. Pathology and differentiation marker analysis of PDMs with conflicting phenotypes. H&E staining of surgical specimens and PDX models derived from the surgical specimens PDX models RP-BL005, -003, and 022.

A major limitation of bulk transcriptome analysis of tumors

Bladder cancer patient derived models enrich tumor cell transcriptome signal

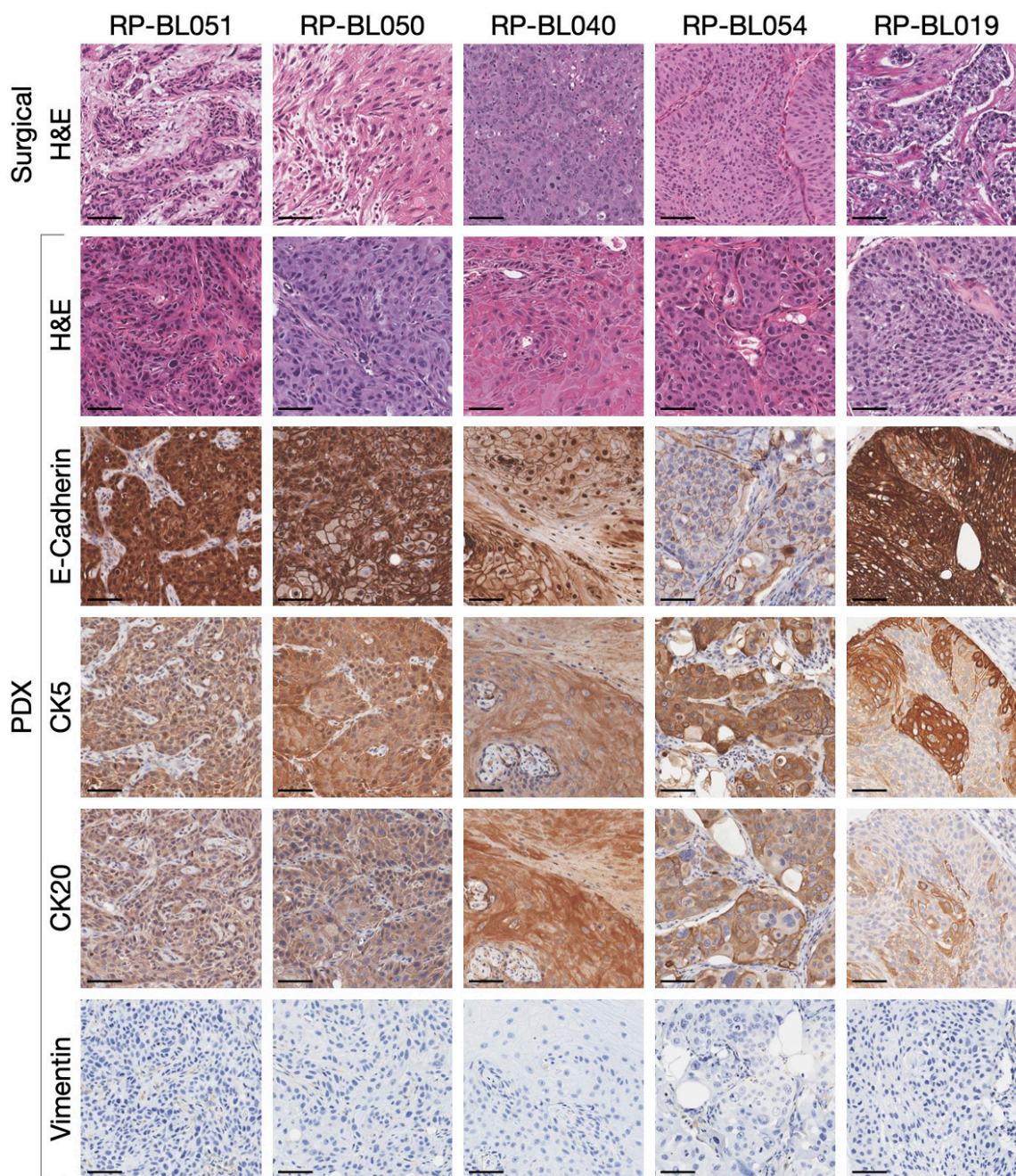


Figure 6. Pathology and differentiation marker analysis of PDMs. H&E staining of surgical specimens and PDX models derived from the surgical specimens PDX models RP-BL0051, 0050, 040, 054 and 019. IHC analysis of PDX models for E-Cadherin, CK5, CK20, and Vimentin. Slides were imaged at 20 \times , Scale Bar =100 μ m.

is that the signal represents an average of the multiple cellular compartments that comprise the tumor [11]. Thus, changes in specific compartments within the tumor are hard to detect, especially compartments that represent a minor component of the tumor such as the stem cell niche. All PDMs enrich the signal from the tumor cell compartment, by reduction of other

cellular compartments, such as the stroma, immune and vasculature. Thus, PDMs can be used to enrich for the tumor cell compartment while reducing the cellular complexity prior to evaluating the transcriptome. Tumor signal is confounded by the heterogeneity in the sample and was such a big problem that informatic methods, including ESTIMATE algorithm, were

invented to address tumor heterogeneity [12]. Here we show that model systems can eliminate that signal obviating the need for additional informatic methods. While these studies focused on transcriptome analysis, future genomic and proteomic studies will further evaluate how closely the PDMs represents the tumor cell compartment.

The advantages of PDXs include their ability to maintain original tumor pathology and to circumvent confounding issues such as altered gene expression that result from serial passage of established cell lines grown on plastic. The PDM models analyzed in these studies are from early passages, and analysis on PDMs at later passages will test if higher passage, stable PDM lines continue to represent the pathology and transcriptome of the original tumor specimen. We demonstrate that PDO and PDS models can be established from a patient's PDX and that such 3D models are still representative of the surgical sample. The growth conditions for PDOs promote differentiation and give rise to the various different cell types within a tumor; thus, PDOs may better reflect the bulk tumor phenotype, relative to other experimental models. Conversely, the PDS assay is often used to enrich for the cancer stem cell population and to evaluate cancer stem cell properties *in vitro* [39-42]. Quantitation of cell viability, sphere number and size following treatment can provide a straightforward readout of therapy effectiveness on the cancer stem cell population. Cancer stem cells are speculated to be a potential source of therapy-resistant cells leading to recurrent disease [43]. Conventional thinking is that the PDS model is the most likely model to contain a high number of cancer stem cells and the least tumor heterogeneity because each sphere is clonally derived. However, we did not see enrichment in the stem cell signature in PDS models. Instead our data showed that PDS models have a higher EMT gene expression profile compared to PDO (**Figure 4A**), indicating that EMT gene expression is elevated in the PDSs supporting a cancer stem cell phenotype as shown previously in spheroid models [34].

The Ba/Sq subtype is molecularly heterogeneous, and molecular subtyping alone is unlikely to fully predict prognosis and treatment response [44]. Only 42% of histologically re-

viewed tumors in Ba/Sq subtype display squamous differentiation, but most tumors with squamous histology are within the Ba/Sq molecular subtype [29]. The papillary morphology was most common in the LumP subtype but was also found in LumNS and LumP [29]. Interestingly, two of the Ba/Sq specimens were able to give rise to both Ba/Sq and Luminal Papillary (LumP) models (RP-BL054 and RP-BL003), whereas both of the LumP specimens only gave rise to LumP models (RP-BL019 and RP-BL022). Recent studies by Kim et al., examined the molecular subtype of PDX models derived from urothelial cancers of the upper urinary tract. Surgical specimens that established PDX models were classified as primarily LumP (82.5%), LumU (8.75%), LumNS (1.25%), Stroma-rich (1.25%), or Ba/Sq (6.25%) [35]. There was histological concordance between the surgical sample and its PDX in 16/17 specimens (94.12%) with a trend toward increased establishment of PDX models from more invasive specimens [35]. Unlike the studies of Kim et al., we did not include upper urinary track surgical specimens. We were more successful at establishing PDX models from Ba/Sq (75% compared to Kim et al. with 6.25%) and we saw no difference in PDX establishment with different stage tumors. The differences in the studies may be due to the differences between these two urothelial cancers or possibly technical differences in establishing PDX models between the two groups. Additionally, organoids established from MIBC had comparable differentiation markers and mutation profiles to the original patient tumor specimen [37]. Interestingly, one surgical specimen with the Stroma-rich molecular subtype resulted in LumP organoids that retained MUC1 expression and were targeted to cell lysis with co-culture with MUC1-targeting CAR-T cells [37]. The ability for robust preclinical studies improves as the number of characterized bladder PDMs increases.

PDX models were characterized based on pathology, molecular subtype, gene expression, and IHC. The RP-BL005 PDX has a sarcomatoid pathology, a Ba/Sq molecular subtype classification and strong staining for E-cadherin and CK5 protein expression, but expresses an EMT gene expression profile (**Figure 4B**) with positive vimentin staining. The RP-BL003 PDX has a squamous differentiation pathology, LumP

molecular subtype classification, high E-cadherin and CK5 staining that confirms the squamous differentiation histopathology, but low expression of CK20 which is inconsistent with the LumP molecular subtype. In addition, RP-BLO03 also had high synaptophysin staining which did not correspond to the histopathology or molecular subtyping. The RP-BLO22 PDX has NE differentiation histopathology, but a LumP molecular subtype with positive IHC staining for E-cadherin and CK20 supporting the LumP molecular subtype and synaptophysin staining supporting the NE histopathology. Analyzing the expression of differentiation markers with IHC can help characterize the PDX models when there is discrepancy between the histopathology and the molecular subtype classification, but tumors express multiple differentiation markers with IHC analysis.

In summary, transcriptomic analysis demonstrated that PDMs were more similar to their surgical specimen than the model type; indicating that the PDMs retained unique features of the tumor from which the PDM was derived. The consensus molecular subtype classification system can be applied to PDMs and demonstrates strong concordance with the classification of the corresponding surgical specimen. Interestingly, of the surgical specimens that established models 75% were Ba/Sq and 25% were LumP molecular subtype. PDMs reduce the complexity of analysis due to tumor heterogeneity while maintaining representation of the tumor cell compartment of the surgical sample from which they were derived.

Acknowledgements

We thank Michelle M. Wrobel for assistance with the PDX models, and Drs. Khurshid Guru and Qiang J. Li for surgical specimen acquisition. This research was funded by the Roswell Park Alliance Foundation and NCI grant P30 CA016056 involving the use of Roswell Park Comprehensive Cancer Center's: Genomic Shared Resource, Experimental Tumor Model Shared Resource, Laboratory Animal Shared Resource, Pathology Network Shared Resource, and Biomedical Research Informatics Shared Resource.

Disclosure of conflict of interest

None.

Address correspondence to: Wendy J Huss, Department of Dermatology, Roswell Park Comprehensive Cancer Center, Elm And Carlton Street, Buffalo 14263, NY, USA. Tel: +01-716-845-1213; E-mail: Wendy.Huss@RoswellPark.org; Barbara A Foster, Department of Pharmacology and Therapeutics, Roswell Park Comprehensive Cancer Center, Elm And Carlton Street, Buffalo 14263, NY, USA. Tel: +01-716-845-1260; E-mail: Barbara.Foster@RoswellPark.org; Kevin H Eng, Department of Cancer Genetics and Genomics, Roswell Park Comprehensive Cancer Center, Elm And Carlton Street, Buffalo 14263, NY, USA. Tel: +01-716-845-6504; E-mail: Kevin.Eng@RoswellPark.org

References

- [1] Siegel RL, Miller KD, Fuchs HE and Jemal A. Cancer statistics, 2021. *CA Cancer J Clin* 2021; 71: 7-33.
- [2] Robertson AG, Kim J, Al-Ahmadie H, Bellmunt J, Guo G, Cherniack AD, Hinoue T, Laird PW, Hoadley KA, Akbani R, Castro MAA, Gibb EA, Kanchi RS, Gordenin DA, Shukla SA, Sanchez-Vega F, Hansel DE, Czerniak BA, Reuter VE, Su X, de Sa Carvalho B, Chagas VS, Mungall KL, Sadeghi S, Pedamallu CS, Lu Y, Klimczak LJ, Zhang J, Choo C, Ojesina AI, Bullman S, Leraas KM, Lichtenberg TM, Wu CJ, Schultz N, Getz G, Meyerson M, Mills GB, McConkey DJ; TCGA Research Network, Weinstein JN, Kwiatkowski DJ and Lerner SP. Comprehensive molecular characterization of muscle-invasive bladder cancer. *Cell* 2017; 171: 540-556, e525.
- [3] Pan CX, Zhang H, Tepper CG, Lin TY, Davis RR, Keck J, Ghosh PM, Gill P, Airhart S, Bult C, Gandara DR, Liu E and de Vere White RW. Development and characterization of bladder cancer patient-derived xenografts for molecularly guided targeted therapy. *PLoS One* 2015; 10: e0134346.
- [4] Skowron KB, Pitroda SP, Namm JP, Balogun O, Beckett MA, Zenner ML, Fayanju O, Huang X, Fernandez C, Zheng W, Qiao G, Chin R, Kron SJ, Khodarev NN, Posner MC, Steinberg GD and Weichselbaum RR. Basal tumor cell isolation and patient-derived xenograft engraftment identify high-risk clinical bladder cancers. *Sci Rep* 2016; 6: 35854.
- [5] Wei L, Chintala S, Ciamporcero E, Ramakrishnan S, Elbanna M, Wang J, Hu Q, Glenn ST, Murakami M, Liu L, Gomez EC, Sun Y, Conroy J, Miles KM, Malathi K, Ramaiah S, Anbarasu A, Woloszynska-Read A, Johnson CS, Conroy J, Liu S, Morrison CD and Pili R. Genomic profiling is predictive of response to cisplatin treatment but not to PI3K inhibition in bladder can-

Bladder cancer patient derived models enrich tumor cell transcriptome signal

- cer patient-derived xenografts. *Oncotarget* 2016; 7: 76374-76389.
- [6] Dutt A, Ramos AH, Hammerman PS, Mermel C, Cho J, Sharifnia T, Chande A, Tanaka KE, Stransky N, Greulich H, Gray NS and Meyerson M. Inhibitor-sensitive FGFR1 amplification in human non-small cell lung cancer. *PLoS One* 2011; 6: e20351.
- [7] Weiss J, Sos ML, Seidel D, Peifer M, Zander T, Heuckmann JM, Ullrich RT, Menon R, Maier S, Soltermann A, Moch H, Wagener P, Fischer F, Heynck S, Koker M, Schottle J, Leenders F, Gabler F, Dabow I, Querings S, Heukamp LC, Balke-Want H, Ansen S, Rauh D, Baessmann I, Altmuller J, Wainer Z, Conron M, Wright G, Russell P, Solomon B, Brambilla E, Brambilla C, Lorimier P, Sollberg S, Brustugun OT, Engel-Riedel W, Ludwig C, Petersen I, Sanger J, Clement J, Groen H, Timens W, Sietsma H, Thunnissen E, Smit E, Heideman D, Cappuzzo F, Ligorio C, Damiani S, Hallek M, Beroukhim R, Pao W, Klebl B, Baumann M, Buettner R, Ernestus K, Stoelben E, Wolf J, Nurnberg P, Perner S and Thomas RK. Frequent and focal FGFR1 amplification associates with therapeutically tractable FGFR1 dependency in squamous cell lung cancer. *Sci Transl Med* 2010; 2: 62ra93.
- [8] Schütte M, Risch T, Abdavi-Azar N, Boehnke K, Schumacher D, Keil M, Yildirim R, Jandrasits C, Borodina T, Amstislavskiy V, Worth CL, Schweiger C, Liebs S, Lange M, Warnatz HJ, Butcher LM, Barrett JE, Sultan M, Wierling C, Golob-Schwarzl N, Lax S, Uranitsch S, Becker M, Welte Y, Regan JL, Silvestrov M, Kehler I, Fusi A, Kessler T, Herwig R, Landegren U, Wienke D, Nilsson M, Velasco JA, Garin-Chesa P, Reinhard C, Beck S, Schäfer R, Regenbrecht CRA, Henderson D, Lange B, Haybaeck J, Keilholz U, Hoffmann J, Lehrach H and Yaspo ML. Molecular dissection of colorectal cancer in pre-clinical models identifies biomarkers predicting sensitivity to EGFR inhibitors. *Nat Commun* 2017; 8: 14262.
- [9] Lee SH, Hu W, Matulay JT, Silva MV, Owczarek TB, Kim K, Chua CW, Barlow LJ, Kandoth C, Williams AB, Berggren SK, Pietzak EJ, Anderson CB, Benson MC, Coleman JA, Taylor BS, Abate-Shen C, McKiernan JM, Al-Ahmadie H, Solit DB and Shen MM. Tumor evolution and drug response in patient-derived organoid models of bladder cancer. *Cell* 2018; 173: 515-528, e517.
- [10] Kamoun A, de Reynies A, Allory Y, Sjudahl G, Robertson AG, Seiler R, Hoadley KA, Groeneveld CS, Al-Ahmadie H, Choi W, Castro MAA, Fontugne J, Eriksson P, Mo Q, Kardos J, Zlotta A, Hartmann A, Dinney CP, Bellmunt J, Powles T, Malats N, Chan KS, Kim WY, McConkey DJ, Black PC, Dyrskjot L, Hognlund M, Lerner SP, Real FX and Radvanyi F; Bladder Cancer Molecular Taxonomy Group. A consensus molecular classification of muscle-invasive bladder cancer. *Eur Urol* 2020; 77: 420-433.
- [11] Morera DS, Hasanali SL, Belew D, Ghosh S, Klaassen Z, Jordan AR, Wang J, Terris MK, Bolag RJ, Merseburger AS, Stenzl A, Soloway MS and Lokeshwar VB. Clinical parameters outperform molecular subtypes for predicting outcome in bladder cancer: results from multiple cohorts, including TCGA. *J Urol* 2020; 203: 62-72.
- [12] Yoshihara K, Shahmoradgoli M, Martínez E, Vegesna R, Kim H, Torres-Garcia W, Treviño V, Shen H, Laird PW, Levine DA, Carter SL, Getz G, Stenke-Hale K, Mills GB and Verhaak RG. Inferring tumour purity and stromal and immune cell admixture from expression data. *Nat Commun* 2013; 4: 2612.
- [13] Yoshida T, Okuyama H, Nakayama M, Endo H, Nonomura N, Nishimura K and Inoue M. High-dose chemotherapeutics of intravesical chemotherapy rapidly induce mitochondrial dysfunction in bladder cancer-derived spheroids. *Cancer Sci* 2015; 106: 69-77.
- [14] Gangavarpu KJ and Huss WJ. Isolation and applications of prostate side population cells based on dye cycle violet efflux. *Curr Protoc Toxicol* 2011; Chapter 22: Unit 22.2.
- [15] DeWard AD, Cramer J and Lagasse E. Cellular heterogeneity in the mouse esophagus implicates the presence of a nonquiescent epithelial stem cell population. *Cell Rep* 2014; 9: 701-711.
- [16] Ge C, Wu S, Wang W, Liu Z, Zhang J, Wang Z, Li R, Zhang Z, Li Z, Dong S, Wang Y, Xue Y, Yang J, Tan Q, Wang Z and Song X. miR-942 promotes cancer stem cell-like traits in esophageal squamous cell carcinoma through activation of Wnt/beta-catenin signalling pathway. *Oncotarget* 2015; 6: 10964-10977.
- [17] Smit JK, Faber H, Niemantsverdriet M, Baanstra M, Bussink J, Hollema H, van Os RP, Plukker JT and Coppes RP. Prediction of response to radiotherapy in the treatment of esophageal cancer using stem cell markers. *Radiother Oncol* 2013; 107: 434-441.
- [18] Dobin A, Davis CA, Schlesinger F, Drenkow J, Zaleski C, Jha S, Batut P, Chaisson M and Gingeras TR. STAR: ultrafast universal RNA-seq aligner. *Bioinformatics* 2013; 29: 15-21.
- [19] Wang L, Wang S and Li W. RSeQC: quality control of RNA-seq experiments. *Bioinformatics* 2012; 28: 2184-2185.
- [20] Li B and Dewey CN. RSEM: accurate transcript quantification from RNA-Seq data with or without a reference genome. *BMC Bioinformatics* 2011; 12: 323.

Bladder cancer patient derived models enrich tumor cell transcriptome signal

- [21] Robinson MD, McCarthy DJ and Smyth GK. edgeR: a Bioconductor package for differential expression analysis of digital gene expression data. *Bioinformatics* 2010; 26: 139-140.
- [22] Smyth GK. Linear models and empirical bayes methods for assessing differential expression in microarray experiments. *Stat Appl Genet Mol Biol* 2004; 3: Article3.
- [23] Kobak D and Berens P. The art of using t-SNE for single-cell transcriptomics. *Nat Commun* 2019; 10: 5416.
- [24] van der Maaten L and Hinton G. Visualizing data using t-SNE. *Journal of Machine Learning Research* 2008; 9: 2579-2605.
- [25] Ritchie ME, Phipson B, Wu D, Hu Y, Law CW, Shi W and Smyth GK. limma powers differential expression analyses for RNA-sequencing and microarray studies. *Nucleic Acids Res* 2015; 43: e47.
- [26] Korotkevich G, Sukhov V and Sergushichev A. Fast gene set enrichment analysis. *bioRxiv* 2019; 060012.
- [27] Liberzon A, Birger C, Thorvaldsdottir H, Ghandi M, Mesirov JP and Tamayo P. The Molecular Signatures Database (MSigDB) hallmark gene set collection. *Cell Syst* 2015; 1: 417-425.
- [28] Subramanian A, Tamayo P, Mootha VK, Mukherjee S, Ebert BL, Gillette MA, Paulovich A, Pomeroy SL, Golub TR, Lander ES and Mesirov JP. Gene set enrichment analysis: a knowledge-based approach for interpreting genome-wide expression profiles. *Proc Natl Acad Sci U S A* 2005; 102: 15545-15550.
- [29] Kamoun A, de Reyniès A, Allory Y, Sjö Dahl G, Robertson AG, Seiler R, Hoadley KA, Groeneveld CS, Al-Ahmadie H, Choi W, Castro MAA, Fontugne J, Eriksson P, Mo Q, Kardos J, Zlotta A, Hartmann A, Dinney CP, Bellmunt J, Powles T, Malats N, Chan KS, Kim WY, McConkey DJ, Black PC, Dyrskjöt L, Höglund M, Lerner SP, Real FX and Radvanyi F; Bladder Cancer Molecular Taxonomy Group. A consensus molecular classification of muscle-invasive bladder cancer. *Eur Urol* 2020; 77: 420-433.
- [30] Jager W, Xue H, Hayashi T, Janssen C, Awrey S, Wyatt AW, Anderson S, Moskalev I, Haegert A, Alshalalfa M, Erho N, Davicioni E, Fazli L, Li E, Collins C, Wang Y and Black PC. Patient-derived bladder cancer xenografts in the preclinical development of novel targeted therapies. *Oncotarget* 2015; 6: 21522-21532.
- [31] Park B, Jeong BC, Choi YL, Kwon GY, Lim JE, Seo SI, Jeon SS, Lee HM, Choi HY and Lee KS. Development and characterization of a bladder cancer xenograft model using patient-derived tumor tissue. *Cancer Science* 2013; 104: 631-638.
- [32] Battle E, Sancho E, Francí C, Domínguez D, Monfar M, Baulida J and García de Herreros A. The transcription factor Snail is a repressor of E-cadherin gene expression in epithelial tumour cells. *Nature Cell Biology* 2000; 2: 84-89.
- [33] Cano A, Pérez-Moreno MA, Rodrigo I, Locascio A, Blanco MJ, del Barrio MG, Portillo F and Nieto MA. The transcription factor Snail controls epithelial-mesenchymal transitions by repressing E-cadherin expression. *Nature Cell Biology* 2000; 2: 76-83.
- [34] Mani SA, Guo W, Liao MJ, Eaton EN, Ayyanan A, Zhou AY, Brooks M, Reinhard F, Zhang CC, Shipitsin M, Campbell LL, Polyak K, Brisken C, Yang J and Weinberg RA. The epithelial-mesenchymal transition generates cells with properties of stem cells. *Cell* 2008; 133: 704-715.
- [35] Kim K, Hu W, Audenet F, Almassi N, Hanrahan AJ, Murray K, Bagrodia A, Wong N, Clinton TN, Dason S, Mohan V, Jebiwott S, Nagar K, Gao J, Penson A, Hughes C, Gordon B, Chen Z, Dong Y, Watson PA, Alvim R, Elzein A, Gao SP, Cocco E, Santin AD, Ostrovnaya I, Hsieh JJ, Sagi I, Pietzak EJ, Hakimi AA, Rosenberg JE, Iyer G, Vargas HA, Scaltriti M, Al-Ahmadie H, Solit DB and Coleman JA. Modeling biological and genetic diversity in upper tract urothelial carcinoma with patient derived xenografts. *Nat Commun* 2020; 11: 1975.
- [36] Ramakrishnan S, Huss W, Foster B, Ohm J, Wang J, Azabdaftari G, Eng KH and Woloszynska-Read A. Transcriptional changes associated with in vivo growth of muscle-invasive bladder cancer cell lines in nude mice. *Am J Clin Exp Urol* 2018; 6: 138-148.
- [37] Yu L, Li Z, Mei H, Li W, Chen D, Liu L, Zhang Z, Sun Y, Song F, Chen W and Huang W. Patient-derived organoids of bladder cancer recapitulate antigen expression profiles and serve as a personal evaluation model for CAR-T cells in vitro. *Clin Transl Immunology* 2021; 10: e1248.
- [38] Cai EY, Garcia J, Liu Y, Vakar-Lopez F, Arora S, Nguyen HM, Lakely B, Brown L, Wong A, Montgomery B, Lee JK, Corey E, Wright JL, Hsieh AC and Lam HM. A bladder cancer patient-derived xenograft displays aggressive growth dynamics in vivo and in organoid culture. *Sci Rep* 2021; 11: 4609.
- [39] Dontu G, Abdallah WM, Foley JM, Jackson KW, Clarke MF, Kawamura MJ and Wicha MS. In vitro propagation and transcriptional profiling of human mammary stem/progenitor cells. *Genes Dev* 2003; 17: 1253-1270.
- [40] Fang DD, Kim YJ, Lee CN, Aggarwal S, McKinnon K, Mesmer D, Norton J, Birse CE, He T, Ruben SM and Moore PA. Expansion of CD133(+) colon cancer cultures retaining stem cell properties to enable cancer stem cell target discovery. *Br J Cancer* 2010; 102: 1265-1275.
- [41] Garraway IP, Sun W, Tran CP, Perner S, Zhang B, Goldstein AS, Hahm SA, Haider M, Head CS, Reiter RE, Rubin MA and Witte ON. Human

Bladder cancer patient derived models enrich tumor cell transcriptome signal

- prostate sphere-forming cells represent a subset of basal epithelial cells capable of glandular regeneration in vivo. *Prostate* 2010; 70: 491-501.
- [42] Wang L, Mezencev R, Bowen NJ, Matyunina LV and McDonald JF. Isolation and characterization of stem-like cells from a human ovarian cancer cell line. *Mol Cell Biochem* 2012; 363: 257-268.
- [43] Dirks P. Cancer stem cells: invitation to a second round. *Nature* 2010; 466: 40-41.
- [44] Warrick JI, Sjödaahl G, Kaag M, Raman JD, Merrill S, Shuman L, Chen G, Walter V and DeGraff DJ. Intratumoral heterogeneity of bladder cancer by molecular subtypes and histologic variants. *Eur Urol* 2019; 75: 18-22.